

# Exotic (anti)ferromagnetism in single crystals of $\text{Pr}_6\text{Ni}_2\text{Si}_3$

Y. Janssen,\* K. W. Dennis, R. Prozorov, P. C. Canfield, and R. W. McCallum

Ames Laboratory DOE and Department of Physics and Astronomy, Iowa State University, Ames, IA 50011, USA

(Dated: October 27, 2018)

The ternary intermetallic compound  $\text{Pr}_6\text{Ni}_2\text{Si}_3$ , is a member of a structure series of compounds based on a triangular structure where the number of Pr atoms in the prism cross section can be systematically varied.  $\text{Pr}_6\text{Ni}_2\text{Si}_3$  contains two distinct Pr lattice sites which result in complex interactions between the magnetic ions. Extensive measurements of specific heat and magnetization on single crystal samples indicate that  $\text{Pr}_6\text{Ni}_2\text{Si}_3$  orders with both a ferromagnet and an antiferromagnet component, with ordering temperatures of 39.6 K and  $\sim 32$  K, respectively. The ferromagnetic component //  $c$ -axis is accompanied by a large hysteresis, and the antiferromagnetic component,  $\perp c$ -axis is accompanied by a spin-flop-type transition. More detailed measurements, of the vector magnetization, indicate that the ferromagnetic and the antiferromagnetic order appear independent of each other. These results not only clarify the behavior of  $\text{Pr}_6\text{Ni}_2\text{Si}_3$  itself, but also of the other members of the structure series,  $\text{Pr}_5\text{Ni}_2\text{Si}_3$  and  $\text{Pr}_{15}\text{Ni}_7\text{Si}_{10}$ .

PACS numbers: 75.50.-y, 75.30.Gw, 75.10.-b

## I. INTRODUCTION

A magnetic system with magnetic moments on non-equivalent crystallographic sites may be difficult to analyze experimentally. Different site symmetries and interatomic spacings can produce magnetic interactions with different signs or strengths as well as different crystalline electric field splittings and even valencies. If, however, the considered magnetic system forms part of a series, similarities in magnetic properties of the members may lead to a greater understanding of the properties of all members. Rare-earth intermetallic compounds often form natural series, because, due to the chemical similarity of rare earths, a particular rare earth can be replaced for another, and the resulting magnetic systematics can be appreciated (See e.g. Ref.1). Another type of series that may be considered is the structure series. In a structure series, structural features are systematically repeated, which may help in understanding the physical properties of members of such series.

In 1984, Parthé and Chabot<sup>3</sup> reviewed the crystal structures of ternary rare-earth (R) transition metal (T) silicide and boride (M) compounds. At that time, about 80 different compositions were known. A number of the R-T-M compounds can be classified as part of a structure series. The majority of these structural series consist of layered structures, and the organization of the layers distinguishes members. However, there are also at least two R-T-M structure series where the basic building block is a triangular prism. These prisms may be assembled into larger prisms in a geometric progression where each member of this progression represents a unique crystal structure with a specific ratio of rare earth to transition metal atoms. The two known series of this type are described by the formulae  $R_{\frac{1}{2}n(n+1)}T_{3(n^2+1)}M_{2n^2+1}$ , with as  $n = 2$  member  $\text{UCo}_5\text{Si}_3$  and  $R_{(n+2)(n+1)}Ni_{n(n-1)+2}Si_{n(n+1)}$ , with as  $n = 2$  member the title compound  $\text{Pr}_6\text{Ni}_2\text{Si}_3$  (Fig. 1). In the former series there is only a single rare earth site so the potential for competing interac-

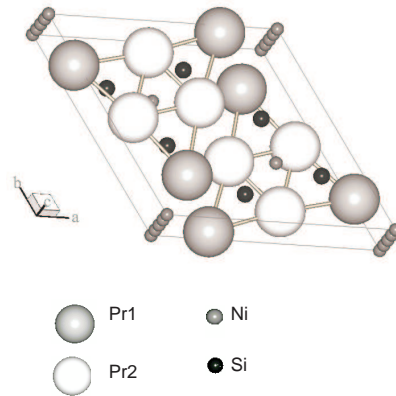


FIG. 1: Schematic drawing<sup>2</sup> of the  $\text{Ce}_6\text{Ni}_2\text{Si}_3$ -type unit cell of  $\text{Pr}_6\text{Ni}_2\text{Si}_3$ .

tions is small. In addition, the low concentration of both rare earth and transition metal ions is expected to result in weak magnetic interactions and low ordering temperatures. On the contrary, the latter series consists of roughly 50 % rare-earth and, moreover, there are different R local environments, see e. g. Ref. 4,5. Furthermore, both the  $n = 3$  and the  $n = 4$  members are known to order magnetically<sup>4,5,6,7</sup>.

In hexagonal  $\text{Pr}_6\text{Ni}_2\text{Si}_3$ , with space group  $P 63/m$ , the Pr ions occupy two independent low-symmetry  $6h$  sites, denoted as Pr1 and Pr2 in Fig. 1. The crystal<sup>3</sup> structures of the other members of the structure series, respectively  $\text{Pr}_5\text{Ni}_2\text{Si}_3$  and  $\text{Pr}_{15}\text{Ni}_7\text{Si}_{10}$ , have the same space group as  $\text{Pr}_6\text{Ni}_2\text{Si}_3$ . In  $\text{Pr}_5\text{Ni}_2\text{Si}_3$ , Pr ions occupy 3 independent  $6h$  sites and one  $2d$  site. In  $\text{Pr}_{15}\text{Ni}_7\text{Si}_{10}$ , Pr ions occupy 5 independent  $6h$  sites. Both  $\text{Pr}_5\text{Ni}_2\text{Si}_3$  and  $\text{Pr}_{15}\text{Ni}_7\text{Si}_{10}$  have Pr ions occupying sites comparable to Pr1 and Pr2

in Fig 1.

Results from polycrystalline samples, for  $\text{Pr}_5\text{Ni}_2\text{Si}_3$  ( $n = 3$ ), or more accurately<sup>5</sup>  $\text{Pr}_5\text{Ni}_{1.9}\text{Si}_3$ , and for  $\text{Pr}_{15}\text{Ni}_7\text{Si}_{10}$  ( $n = 4$ ) indicate that both compounds order ferromagnetically<sup>4</sup>, at  $\sim 50$  K, and at  $\sim 60$  K, respectively. For both  $\text{Pr}_5\text{Ni}_2\text{Si}_3$  and  $\text{Pr}_{15}\text{Ni}_7\text{Si}_{10}$  the specific heat shows, besides the anomaly due to the Curie temperature, another, weaker, anomaly, at  $\sim 27$  K and at  $\sim 33$  K, respectively. For both these compounds, at temperatures below the low-temperature specific-heat anomaly, the magnetization isotherms show the development of a significant coercivity. Moreover, there occurs evidence of metamagnetic-like transitions close to 3 T for  $\text{Pr}_5\text{Ni}_2\text{Si}_3$  at 5 K, and close to 4 T for  $\text{Pr}_{15}\text{Ni}_7\text{Si}_{10}$  at 5 K.

In this paper, we report on the magnetic properties of solution-grown, single-crystalline  $\text{Pr}_6\text{Ni}_2\text{Si}_3$ , the  $n = 2$  member of the aforementioned structure series. Results of specific heat, and of extensive anisotropic magnetization measurements are presented. Moreover, measurements of the magnetization vector have been used to clarify the low-temperature magnetic order, which following crystallographic nomenclature<sup>8</sup> appears to be 'exotic'. Finally, the results are discussed within the systematics seen also for the  $n = 3$  and  $n = 4$  members of the series.

## II. EXPERIMENTAL

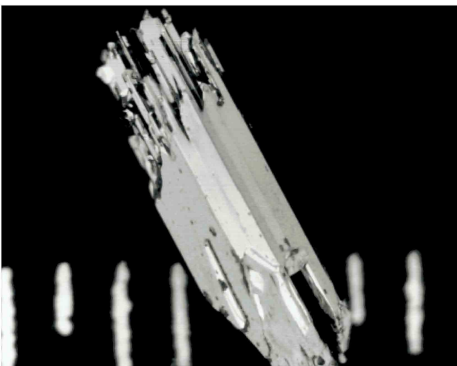


FIG. 2: Photograph of a self-flux grown crystal of  $\text{Pr}_6\text{Ni}_2\text{Si}_3$ , on a background with a  $mm$ -scale. The crystal axis is the  $c$  axis, and a  $[110]$  facet is facing the reader.

Single crystals of  $\text{Pr}_6\text{Ni}_2\text{Si}_3$  were grown out of a high-temperature ternary solution<sup>9,10,11</sup>. An initial alloy composition and a useful temperature range for growth were determined by means of combined DTA and growth experiments<sup>12</sup>. The initial alloy composition used was  $\text{Pr}_{60}\text{Ni}_{25}\text{Si}_{15}$ , and the useful temperature range for

growth was determined to be between  $\sim 1000^\circ\text{C}$  and  $\sim 880^\circ\text{C}$ . The starting elements were sealed in a 3-cap Ta crucible<sup>11</sup>, that was sealed in an evacuated quartz ampoule. The ampoule was initially heated up to  $\sim 1200^\circ\text{C}$ , to ensure a well-homogenized alloy, cooled to  $1000^\circ\text{C}$  at  $\sim 50^\circ\text{C}/\text{h}$ , and then cooled down to  $880^\circ\text{C}$  at  $3^\circ\text{C}/\text{h}$ . The ampoule was taken out of the furnace, inverted and centrifuged, resulting in a separation of crystals from an excess liquid. Crystals have a hexagonal-prismatic growth habit with faces parallel to the  $[001]$  crystallographic direction, and normal to the  $[110]$  direction<sup>13</sup>. The crystals were up to 10 mm long, and had effective diameters of up to 1 mm. A photograph of a  $\text{Pr}_6\text{Ni}_2\text{Si}_3$  crystal is displayed in Fig. 2.

For initial characterization, we measured a powder x-ray diffraction pattern on finely ground crystals from the growth yield with a Rigaku Miniflex+ diffractometer employing Cu-K $\alpha$  radiation. The pattern was analyzed with Rietica<sup>14</sup>, using a Le Bail-type<sup>15</sup> refinement, and it was indexed according to the space group P63/m, with lattice parameters  $a = 11.96(2)$  Å and  $c = 4.27(1)$  Å. These results are consistent with those for isostructural<sup>16</sup>  $\text{Ce}_6\text{Ni}_2\text{Si}_3$ , which has somewhat larger lattice parameters ( $a=12.11$  Å, and  $c=4.32$  Å), consistent with lanthanide contraction.

Specific heat was determined in a Quantum Design physical property measurement system (QD-PPMS) at temperatures between 2 K and 70 K. Magnetization measurements were performed using Quantum Design magnetic property measurement system magnetometers (QD-MPMS), in magnetic fields up to 5 T, and at temperatures between 5 K and 300 K. For most of the experiments described below, only the magnetization component parallel to the applied field was measured for samples aligned with the applied field parallel and perpendicular to the hexagonal  $c$ -axis. To investigate a possible in-plane magnetic anisotropy the sample was aligned with the field perpendicular to the  $c$ -axis, and rotated by means of a horizontal-axis rotator around the  $c$ -axis.

Generally, a magnetization vector can be decomposed into three perpendicular vector components. We can distinguish a longitudinal component, along the applied field direction, here called  $M_L$ , and transverse components in the plane perpendicular to the applied field, here called  $M_X$  and  $M_Y$ . We used a QD-MPMS-5 system, which was equipped with both a conventional longitudinal pick-up-coil system and a transverse pick-up-coil system. Since the magnetometer is equipped with one single transverse pick-up-coil system, we used the vertical-axis sample rotator to determine both the  $M_X$  and the  $M_Y$  components of magnetization. For these vector measurements, the sample was aligned with the unique  $c$ -axis at an angle of about 60 degrees with the applied field direction.

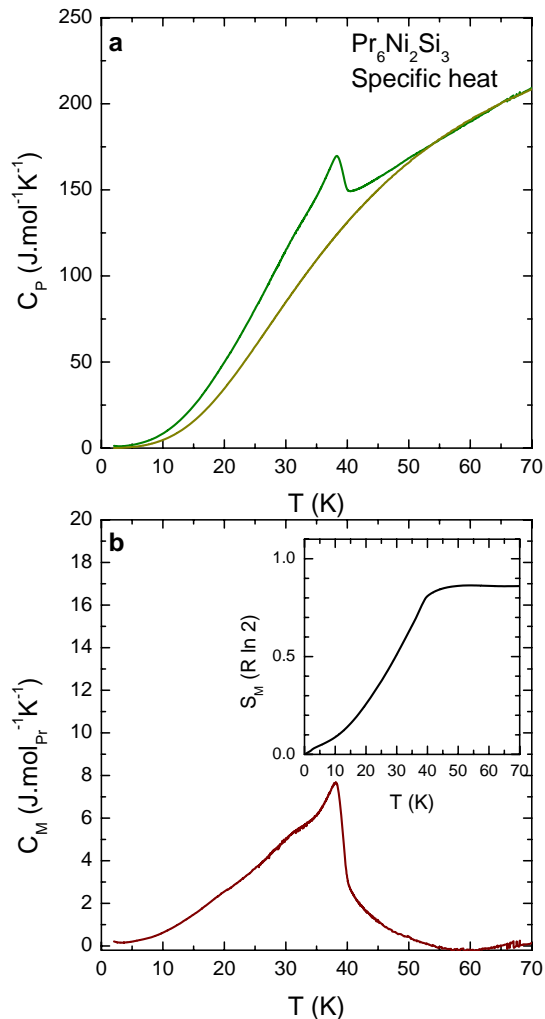


FIG. 3: (Color online) **a** Zero-field specific heat  $C_p$  as a function of temperature, also included is an estimate of the lattice specific heat. The mean-field-like with an onset near  $T = 40$  K is close to the Curie temperature. **b** Magnetic specific heat per Pr ion obtained from **a**. Note the shoulder between 30-35 K. The inset shows the estimated magnetic entropy to reach values close to  $R \ln 2$  at the ordering temperature.

### III. RESULTS

Temperature-dependent specific heat is presented in Fig. 3a. It will be shown below that  $\text{Pr}_6\text{Ni}_2\text{Si}_3$  orders ferromagnetically. Then an onset criterion<sup>17</sup> for a peak in specific heat can be used. The peak in specific heat shows an onset temperature close to 40 K. A lattice contribution to specific heat, also shown, was estimated according to the Debye model, and we obtained a Debye temperature of  $\Theta_D \approx 165$  K. An electronic contribution was ignored. An estimate, Fig. 3b, for the magnetic con-

tribution per Pr ion  $C_M$  was obtained by subtracting this lattice contribution from the measured specific heat. Notice that, besides the peak near 40 K, also a shoulder with a maximum around 30 K can be observed. The temperature-dependent magnetic entropy  $S_M$ , estimated by integrating  $C_M/T$  up to 70 K and displayed in the inset of Fig. 3 b, saturates at a value close to  $R \ln 2$  at 40 K, and then remains approximately constant up to 70 K. This indicates that, averaged over the two crystallographically distinct Pr ions, a pair of well-isolated singlet states, or a doublet ground state, is responsible for the magnetic order in this compound.

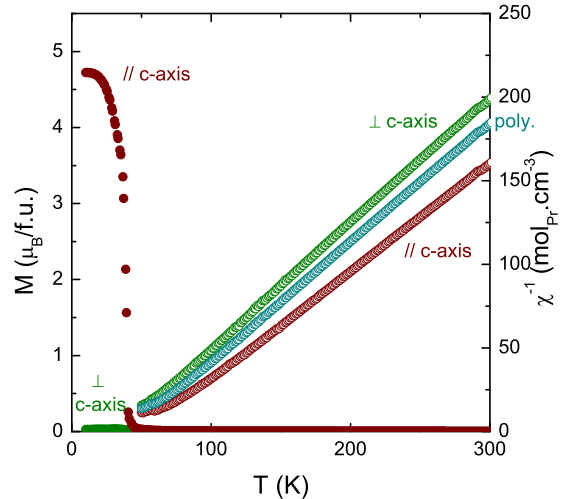


FIG. 4: (Color online) Closed circles, left axis:  $\text{Pr}_6\text{Ni}_2\text{Si}_3$  temperature-dependent magnetization measured in 0.01 T, both for  $H // c$ -axis (top) and for  $H \perp c$ -axis (bottom). Open circles, right axis: temperature-dependent inverse differential susceptibility determined for  $H // c$ -axis (bottom) and  $H \perp c$ -axis (top) together with polycrystalline average  $\chi^{-1}$  (center).

Fig. 4 shows temperature-dependent magnetization measured upon cooling in a field of 0.01 T applied both parallel and perpendicular to the  $c$ -axis. Two features are immediately obvious: the magnetization parallel to the  $c$ -axis indicates a ferromagnetic component  $// c$ -axis below  $\sim 40$  K, and the magnetization  $\perp c$ -axis is much smaller than the magnetization parallel to the  $c$ -axis, especially below 40 K, which indicates that the magnetic anisotropy in this compound is very large and favors the moments to align themselves parallel to the  $c$ -axis.

Temperature-dependent magnetization for both these sample alignments was determined in various fields up to 5 T. From these it was found that above 50 K the magnetization for both alignments increases linearly with increasing fields, thus a differential magnetic susceptibility  $\chi_{\text{diff}} = \frac{\Delta M}{\Delta H}$  could be determined. A polycrystalline aver-

age was obtained by averaging  $\chi // c$ -axis and  $\chi \perp c$ -axis according to  $\chi_{avg} = (\chi_{//} + 2\chi_{\perp})/3$ .

Fig.4 also shows the inverted temperature-dependent differential magnetic susceptibilities  $// c$ -axis,  $\perp c$ -axis and polycrystalline average. All three are linear, though not parallel, with temperature above 100 K, thus can be described by a Curie-Weiss law. The effective moments calculated for  $\chi_{avg}$ ,  $\chi_{//}$ , and  $\chi_{\perp}$  equal  $3.35 \mu_B/\text{Pr}$ ,  $3.50 \mu_B/\text{Pr}$ , and  $3.26 \mu_B/\text{Pr}$ , which are all not too far from the theoretical free-ion value for Pr ( $3.58 \mu_B$ ), thus indicating that the magnetism in  $\text{Pr}_6\text{Ni}_2\text{Si}_3$  is determined by Pr local magnetic moments. However, the fact that the calculated effective moments are different for the different crystallographic directions is an indication of a substantial crystal-field splitting of the  $2J+1$  levels of the Pr-4f shell, which is still noticeable at room temperature. Weiss temperatures  $\Theta$  of 41 K, 53 K, and 33 K were found for  $\Theta_{avg}$ ,  $\Theta_{//}$ , and  $\Theta_{\perp}$ , respectively, positive values which are reasonably close to  $T_C$ , and which indicate (mainly) ferromagnetic interactions between the Pr moments.

### A. $H // c$ -axis

The Curie temperature for the onset of ferromagnetic order  $// c$ -axis can be determined from Arrott plots<sup>18</sup>. Fig. 5 shows such plots for  $\text{Pr}_6\text{Ni}_2\text{Si}_3$ , obtained from magnetization isotherms  $H // c$ -axis in fields up to 500 Oe. In Arrott's original paper<sup>18</sup>, plots of  $M^3$  vs  $H$  are used rather than the more conventional  $M^2$  vs  $H/M$ . According to Arrott's criterion, precisely at  $T_C$ , the magnetic susceptibility  $\chi$  tends to infinity, causing terms of  $M^3$  to be dominant at low enough  $H$ . In other words, the Curie temperature is at that temperature where  $H$ -dependent  $M^3$  is exactly linear starting at  $H = 0$ . A criterion for the linearity of a fit line is given by the regression factor  $R$ , which ranges between 0 and 1, where 1 indicates a perfect line. The top panel of Fig. 5 shows  $M^3$  vs  $H$  taken at temperatures between 39 K and 40 K, and the inset to that panel shows the temperature-dependent  $R$  of such linear fits. From this the Curie temperature is determined as  $T_C = 39.6$  (1) K. This value agrees very well with the above obtained value for the onset of the specific heat peak. For completeness, a more conventional Arrott plot of  $M^2$  vs  $H/M$  is displayed in the bottom panel of Fig. 5. As expected, the curve taken at 39.6 K extrapolated to zero  $M^2$  is closest to intercepting the  $H/M$  axis.

Hysteretic behavior of  $\text{Pr}_6\text{Ni}_2\text{Si}_3$  at 1.8 K for  $H // c$ -axis is shown in Fig. 6. These results were obtained by cooling the aligned crystal in zero field and measuring first the virgin magnetization curve. The observed presence of high coercivity in conjunction with the small slope of the virgin curve can be taken as a signature of the presence of narrow domain walls<sup>19,20,21,22,23</sup>. Such narrow walls can be strongly pinned by magnetic obstacles of atomic dimensions. The strong increase of the magnetization on the virgin curve at  $H_P = 0.45$  T marks the

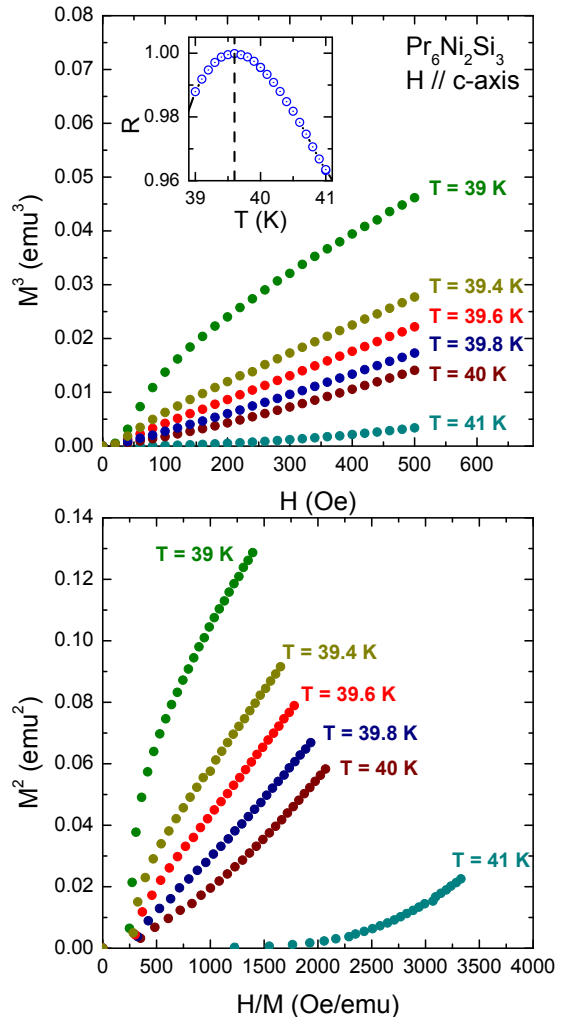


FIG. 5: (Color online)  $\text{Pr}_6\text{Ni}_2\text{Si}_3$  Arrott plots for  $H // c$ -axis. The upper panel shows field ( $H$ ) dependent magnetization ( $M^3$ ) for representative temperatures. The inset shows the  $T$ -dependent regression factor  $R$  for a linear fit through  $M^3(T)$ , indicating the Curie temperature  $T_C = 39.6(1)$  K. The lower panel shows conventional Arrott plots, of  $M^2$  vs.  $H/M$  of the same data sets.

propagation field  $H_P$  at which the external field is able to detach the narrow walls from the pinning sites. At higher fields the walls are removed from the crystal. Upon decreasing the fields from 1 T into the region of negative fields, reversed domains and domain walls can nucleate but the movement of these walls is impeded by the pinning sites so that the reversed domains cannot grow. This becomes possible again only for negative fields equal in magnitude to  $H_P$ , causing the absolute value of the coercive field to be equal to the propagation field,  $H_C = H_P$ .

Because of the strong hysteresis, the spontaneous mag-

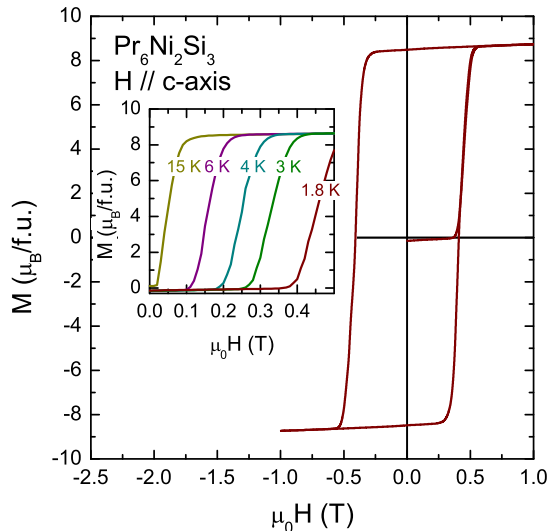


FIG. 6: (Color online)  $\text{Pr}_6\text{Ni}_2\text{Si}_3$  zero-field-cooled magnetization loop for  $H // c$ -axis at 1.8 K. The inset shows the development of virgin magnetization with temperature, demonstrating the coercive behavior.

netization  $M_S$  at 1.8 K can directly be obtained from this Figure. It equals about  $8.5 \mu_B/\text{f.u.}$ , amounting to about  $1.4 \mu_B/\text{Pr}$  ion, which is much lower than the free-ion value of  $3.2 \mu_B/\text{Pr}$ , which may be related to strong crystal-electric field effects and the low point symmetry of both Pr-crystallographic sites.

The temperature dependence of the coercive field is demonstrated in the inset of Fig. 6, which shows virgin  $M(H)$  at different temperatures below 15 K. Note that besides having a different coercive field these curves overlap, so  $M_S$  is almost temperature independent below 15 K.

Measurements at various temperatures below  $T_C$  indicate the same behavior as at 1.8 K, but with a strongly temperature-dependent  $H_C$ . Fig. 7 shows temperature-dependent  $H_C$ . According to a model proposed by Barbara and Uehara<sup>22</sup>, the temperature dependence of coercivity can be described as:

$$H_C^{-1}(T) = H_C(0)^{-1} + \alpha T, \quad (1)$$

where  $\alpha$  is proportional to the spontaneous magnetization divided by the domain-wall energy,  $\alpha \propto M_S/\gamma^2$ .  $\gamma^2$  in turn is proportional to the product of the average exchange energy and the average anisotropy energy. The inset of Fig. 7 shows temperature-dependent  $H_C^{-1}$  at temperatures between 1.8 K and 15 K. A very good fit to this line is given by a second-order polynomial, and when comparing to Eq. 1, this means that  $\alpha$  is linearly dependent on  $T$ . Values found are:  $H_C(0)^{-1} = 1.4(3)$

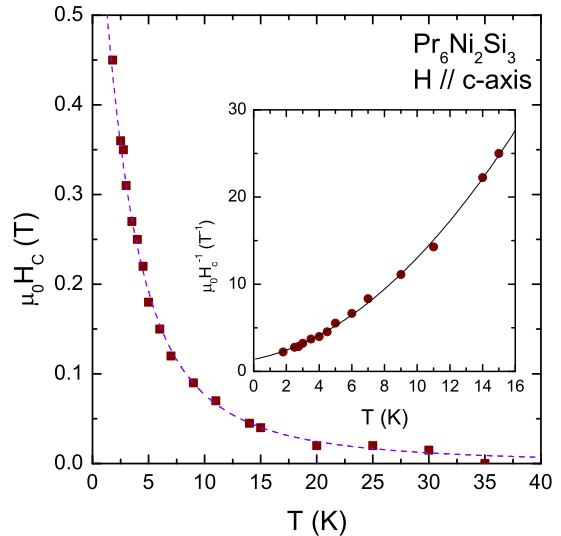


FIG. 7: (Color online)  $\text{Pr}_6\text{Ni}_2\text{Si}_3$  temperature-dependent coercive field for  $H // c$ -axis. The line is obtained as described in the text.

$T^{-1}$ , and  $\alpha(T) = 0.37(9) + 0.079(6)T$ , leading to a zero-temperature  $H_C$  of 0.71 T. The dotted line in the main Fig. 7 was calculated using these values.

Since  $M_S$  is constant below 15 K,  $M_S$  is not expected to contribute to variations of  $\alpha(T)$  below 15 K. Therefore, the variations in  $\alpha$  below 15 K have to be proportional to the variations of  $1/\gamma^2$ , the inverted product of the average exchange energy and the average anisotropy energy. Both the exchange energy and the anisotropy energy may be expected to decrease with increasing temperature, leading to  $\alpha$  growing with increasing temperature.

## B. $H \perp c$ -axis

Fig. 8 shows temperature-dependent magnetization for  $H \perp c$ -axis measured, with temperature decreasing, in various fields up to 5 T. In 0.01, 1 and 2 T, the magnetization shows a maximum, which appears close to 32 K, for 0.01 T and 1 T, and close to 27 K for 2 T. In 3 T and higher, no maximum is observed. Such behavior, a maximum in temperature-dependent magnetization, which shifts to lower temperature with increasing field strengths, is common in antiferromagnets<sup>24</sup>. Note also that the maximum in the 0.01 T curve occurs at a temperature close to the 32 K shoulder in specific heat.

Field-dependent magnetization isotherms for  $H \perp c$ -axis at temperatures between 5 K and 45 K are shown in Fig. 9. At 5 K, starting in zero field, the magnetization starts at zero and first increases weakly and linearly with



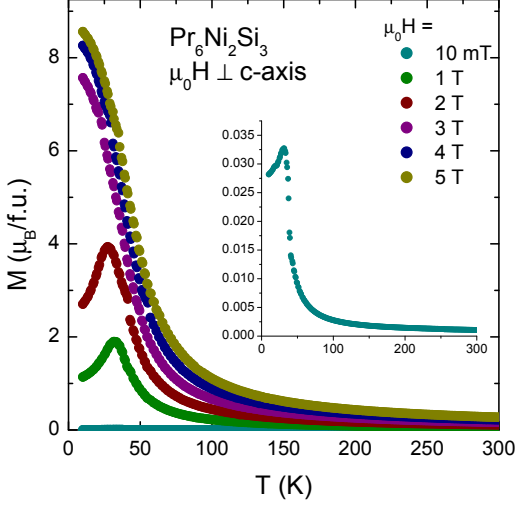


FIG. 8: (Color online) Temperature-dependent magnetization for  $H \perp c$ -axis measured in various fields up to 5 T. Note the maxima for 0.01 ( $\approx 32$  K), 1 ( $\approx 32$  K), and 2 T ( $\approx 27$  K).

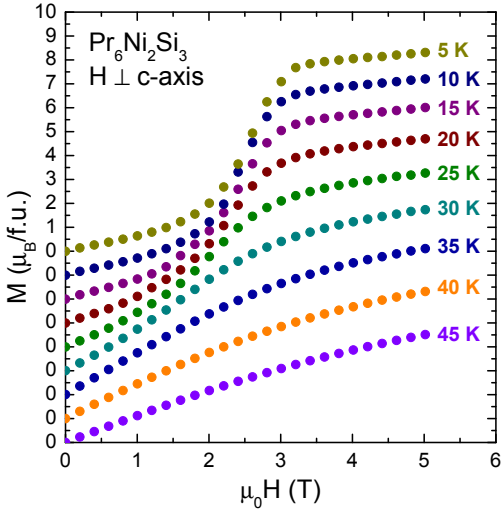


FIG. 9: (Color online) Field-dependent magnetization of  $\text{Pr}_6\text{Ni}_2\text{Si}_3$  at various temperatures measured with  $H \perp c$ -axis. For clarity, the curves have been shifted by  $1 \mu_B/\text{f.u.}$  with respect to one another.

increasing field. Close to 2 T, the magnetization starts to increase much faster with increasing field, a process

which ends close to 3 T, above which the magnetization continues to increase linearly with increasing field, at a slope similar to the slope in low field. As temperature increases, this process becomes less pronounced, resulting in a weakly s-shaped magnetization at 30 K, and a featureless magnetization at 35 K and higher. Also these results are consistent with the magnetization of a simple antiferromagnet, and the magnetization process could be interpreted as due to a spin flop<sup>24</sup>.

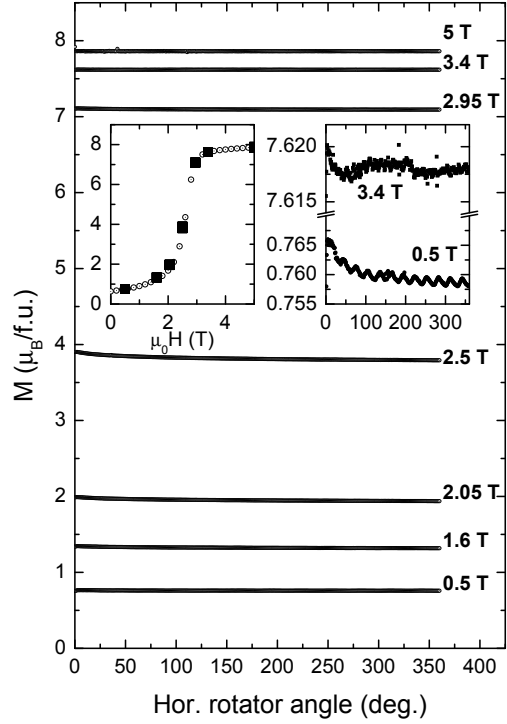


FIG. 10:  $\text{Pr}_6\text{Ni}_2\text{Si}_3$  horizontal-angle dependent magnetization, measured at 5 K, in various fields ( $H \perp c$ -axis) up to 5 T. The left inset shows all data as a function of  $H$ , superimposed on a denser dataset measured at zero angle. The right inset shows a zoom in of the 0.5 T data (bottom) and the 3.4 T data (top).

To determine magnetic anisotropy in the plane perpendicular to the  $c$ -axis we more precisely measured the magnetization at 5 K for the field  $\perp c$ -axis with a horizontal rotator, rotating the sample around the  $c$ -axis. In a hexagonal system with a very strong in-plane anisotropy, the in-plane magnetization may vary by as much as  $1 - \cos 30^\circ \sim 15\%$ . Fig. 10 shows the magnetization in various fields up to 5 T, measured at horizontal rotator angles between 0 and  $360^\circ$ . For all chosen field strengths, the variation in magnetization is smaller than the symbols used for the figure. The in-plane anisotropy of  $\text{Pr}_6\text{Ni}_2\text{Si}_3$  in fields up to 5 T is thus very small, which is exemplified in the left inset, by plotting all thus measured magnetization values on a more densely measured

field-dependent magnetization curve, measured at zero angle. Strongly zoomed in, see right inset of Fig. 10, egthe magnetization at 0.5 T shows a very weak and 12 fold variation, with an amplitude of variation of about 0.1 %. This variation disappears in higher fields: the zoomed in angular dependent magnetization measured in 3.4 T shows no such variation. This 12 fold variation may be related to the two crystallographically distinct magnetic Pr sites in the unit cell of  $\text{Pr}_6\text{Ni}_2\text{Si}_3$ .

### C. $H$ applied at $60^\circ$ from the $c$ -axis

The crystal was mounted and centered in a straw such that the applied field  $H$  made an angle of  $\approx 60^\circ$  with the  $c$ -axis. The very weak in-plane anisotropy, Fig. 10, made it clear that no particular attention to the planar direction closest to the applied field was necessary, which is not true if the in-plane anisotropy is strong<sup>25</sup>. The sample was then cooled in an applied field of 5 T from room temperature to 5 K, at which temperature the field was removed. Vertical-rotator angle-dependent zero-field magnetization measured both parallel (longitudinal magnetization  $M_L$ ) and perpendicular to  $H$  (transverse magnetization  $M_T$ ) are shown in Fig. 11. Whereas the measured  $M_L$  is vertical-angle independent,  $M_T$  is determined as the amplitude of the measured transverse magnetization cosine. We thus find for  $M_T$  a value of  $\approx 7.5\mu_B/\text{f.u.}$  and for  $M_L$   $3.8\mu_B/\text{f.u.}$  The angle of the magnetic moment with the applied field is given by  $\tan^{-1}\frac{M_T}{M_L} = 63^\circ$ , which is in good agreement with the angle at which the crystal axis was mounted in the sample holder. The size of the moment vector  $|M| = \sqrt{M_L^2 + M_T^2} = 8.4\mu_B/\text{f.u.}$  is in excellent agreement with the magnetization moment found at 5 K for  $H \parallel c$ -axis.

Field-dependent magnetization was determined by measuring both  $M_L$  and  $M_T$  at 5 K in various  $H$  up to 5 T.  $M_L$  was determined in the conventional way. Full rotations of the vertical rotator, similar to the measurement shown in Fig. 11, were made to determine  $M_T$ . In this way, we verified that the magnetic moment does not rotate in the plane perpendicular to the magnetic field, which was a distinct possibility<sup>25</sup>. The results are shown in Fig 12. As expected,  $M_L$  increases uniformly with increasing  $H$ , and the spin-flop-like transition starts close to 2.5 T, a field some 15% ( $=1/\sin 60^\circ$ ) higher than for the measurement shown in Fig. 9. At the same time,  $M_T$  decreases uniformly with increasing fields, which generally indicates a rotation of the magnetic moment towards  $H$ . The spin-flop-like transition for this magnetization-vector component mimics the one for  $M_L$ , but as a stronger decrease rather than an increase. The amount by which the magnetization vector decreases for  $M_T$  due to the spin-flop-like transition may seem small compared to the increase observed for  $M_L$ . This is clarified examining the total magnetization, the vector sum  $|M|$ , also shown in Fig. 12.  $|M|$  shows a

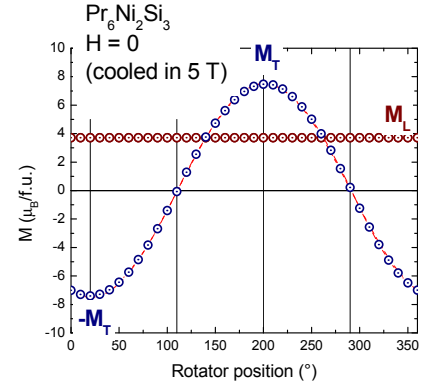


FIG. 11:  $\text{Pr}_6\text{Ni}_2\text{Si}_3$  zero-field magnetization, measured at 5 K both parallel to the applied field  $H$  ( $M_L$ ) and perpendicular to it ( $M_T$ ) as a function of (vertical) rotator position. This was measured on a field-cooled sample which was mounted with its  $c$ -axis at an angle of approx. 60 degrees with  $H$ .

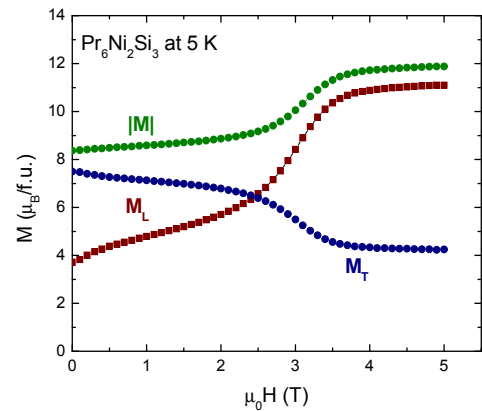


FIG. 12:  $\text{Pr}_6\text{Ni}_2\text{Si}_3$  field-dependent magnetization, measured at 5 K both parallel ( $M_L$ ) and perpendicular ( $M_T$ ) to the applied field, resulting in a vector-summed magnetization  $|M|$ .

small, linear increase with increasing field strenghts up to  $\sim 2.5$  T, and increases even further during the spin-flop-like transition, up to about 3.5 T, above which it further increases slightly and linearly. This anomalous change in length of the magnetization vector is an immediate indication that the metamagnetic spin-flop-like transition for  $H \perp c$ -axis is not due to a simple rotation of the magnetization vector<sup>25</sup>.

The lower panel of Fig. 13 shows the measured field-dependent magnetization vector with the field applied

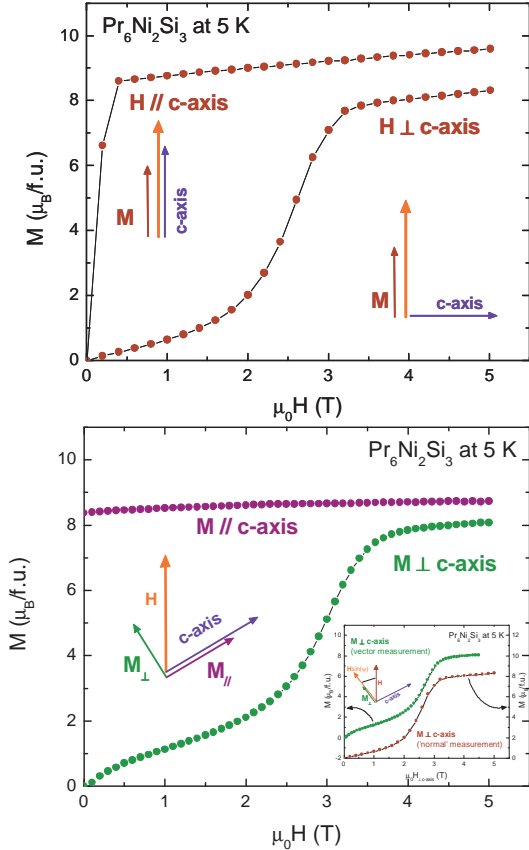


FIG. 13:  $\text{Pr}_6\text{Ni}_2\text{Si}_3$  field-dependent magnetization, measured at 5 K both parallel ( $M_L$ ) and perpendicular ( $M_T$ ) to the applied field, resulting in a vector-summed magnetization  $|M|$ .

at  $\sim 60^\circ$  from  $c$ -axis (Fig. 12) decomposed<sup>25</sup> in a component  $// c$ -axis and a component  $\perp c$ -axis. For comparison, field-dependent longitudinal magnetization measured with  $H$  applied  $// c$ -axis and with  $H$  applied  $\perp c$ -axis are shown in the upper panel of Fig. 13. In both the lower and upper panel, we show an almost constant magnetization  $// c$ -axis, whereas the magnetization  $\perp c$ -axis shows a spin-flop like transition. The inset of the lower panel of Fig. 13 shows the magnetization  $\perp c$ -axis obtained by vector magnetometry with  $H$  projected  $\perp c$ -axis, compared to the longitudinal magnetization from the upper panel of Fig. 13. Thus the spin-flop like process  $\perp c$ -axis occurs independent from the magnetization  $// c$ -axis, and is only due to the  $H \perp c$ -axis.

#### IV. DISCUSSION AND CONCLUSIONS

The experimental results shown above indicate quite clearly that the magnetic order in the intermetallic compound  $\text{Pr}_6\text{Ni}_2\text{Si}_3$  has both ferromagnetic and antiferromagnetic components, which may be called 'exotic' fol-

lowing proposed nomenclature<sup>8</sup>. As described below, it may well be that the ferromagnetic order mainly involves one of the two Pr sites, and the antiferromagnetic order the other. In our view, two magnetic phase transitions may be discerned, possibly with different propagation vectors,  $q=0$  for the ferromagnetic order and another one for the antiferromagnetic order. The first transition occurs at  $T_C = 39.6$  K, where Pr moments order ferromagnetically  $// c$ -axis, with a spontaneous magnetization substantially lower than the theoretical free-ion moment for Pr. This transition is evidenced by a clear specific heat anomaly and by Arrott plots of  $M(H)$  for  $H // c$ -axis. The second magnetic transition is due to antiferromagnetic order  $\perp c$ -axis and shows as a weak shoulder in specific heat close to 32 K, and in low fields  $\perp c$ -axis by  $M(T)$ , where a peak occurs close to 32 K. Furthermore, spin-flop-like transitions are only clearly observed below 32 K.

The ferromagnetic order  $// c$ -axis is further corroborated by the strong and strongly temperature-dependent coercivity that occurs for  $M // c$ -axis, which shows itself in nearly square magnetization loops at low temperatures. Such loops occur in ferromagnets with narrow domain walls which are strongly pinned, on obstacles of atomic size. The coercivity in  $\text{Pr}_6\text{Ni}_2\text{Si}_3$  becomes stronger with decreasing temperatures, which may be expected for any coercive magnet. We find no clear evidence that the behavior of the coercive field is related to the development of antiferromagnetic order  $\perp c$ -axis. The cause of the narrow domain walls, which are not usually observed in pure single crystals is not presently clear, but may be related to the intrinsic crystallographic disorder we have found<sup>13</sup>.

The antiferromagnetic order  $\perp c$ -axis in turn is corroborated by a magnetization process, similar to a spin-flop transition, which starts close to 2 T at 2 K for  $H \perp c$ -axis. That this magnetization process is only due to magnetization for  $H \perp c$ -axis is evidenced by measurements of the magnetization vector for  $H$  applied at an angle of  $60^\circ$  with the  $c$ -axis. Although the fact that  $M_S // c$ -axis is substantially smaller than the full free-ion Pr moment enables additional magnetic order, there is no evidence that here these two magnetic orderings  $// c$ -axis and  $\perp c$ -axis are linked.

The magnetic properties of single-crystalline  $\text{Pr}_6\text{Ni}_2\text{Si}_3$  is consistent with the magnetic properties of the other members of the structure series,  $\text{Pr}_5\text{Ni}_2\text{Si}_3$  and  $\text{Pr}_{15}\text{Ni}_7\text{Si}_{10}$ , which order also ferromagnetically at 50 and at 60 K, respectively. Both these compounds also show, besides the Curie-temperature anomaly, shoulders in specific heat, at 27 K and at 33 K, respectively, below which temperatures for both these compounds in the polycrystalline, magnetization metamagnetic-like behavior appears.

Preliminary studies on single crystals<sup>26</sup> of these compounds indicate that they also order ferromagnetically  $// c$ -axis and antiferromagnetically  $\perp c$ -axis. Furthermore, a preliminary neutron powder diffraction<sup>27</sup> mea-



surement of  $\text{Pr}_5\text{Ni}_2\text{Si}_3$ , indicated that Pr moments order ferromagnetically //  $c$ -axis, and the moment on the site comparable to Pr1 in Fig. 1 has a small moment //  $c$ -axis compared to the other Pr sites. Also, a separate incommensurate diffraction peak was found at low temperature, which we assume is due to antiferromagnetic order mainly on this crystallographic site.

Concluding, the above presented results on  $\text{Pr}_6\text{Ni}_2\text{Si}_3$  indicate that its ordered state manifests both ferromagnetic and antiferromagnetic components. The results are not only consistent with results obtained on other members of the structure series of which it forms part, but

also clarifies these.

## V. ACKNOWLEDGMENTS

We are indebted to S. L. Bud'ko, Y. Mozharivskyj, and J. Frederick for valuable discussions and for help with the experiments. Work at the Ames Laboratory was supported by the Department of Energy, Basic Energy Sciences under Contract No. DE-AC02-07CH11358.

- 
- \* Present address: Brookhaven National Laboratory, Upton, NY 11973, USA; yjanssen@bnl.gov
- <sup>1</sup> K. N. R. Taylor, *Adv. Phys.* **20**, 551 (1971).
  - <sup>2</sup> T. C. Ozawa and S. J. Kang, *J. Appl. Cryst.* **37**, 679 (2004).
  - <sup>3</sup> E. Parthé and B. Chabot, in *Handbook on the Physics and Chemistry of Rare Earths*, edited by K. A. Gschneidner, Jr. and L. Eyring (North-Holland, Amsterdam, 1984), vol. 6, p. 113.
  - <sup>4</sup> D. C. Jiles, S. H. Song, J. E. Snyder, V. K. Pecharsky, T. A. Lograsso, D. Wu, A. O. Pecharsky, Y. Mudryk, K. W. Dennis, and R. W. McCallum, *J. Magn. Magn. Mater.* **299**, 288 (2006).
  - <sup>5</sup> A. O. Pecharsky, Y. Mozharivskyj, K. W. Dennis, K. A. Gschneidner, R. W. McCallum, G. J. Miller, and V. K. Pecharsky, *Phys. Rev. B* **68**, 134452 (2003).
  - <sup>6</sup> S. H. Song, D. C. Jiles, J. E. Snyder, A. O. Pecharsky, D. Wu, K. W. Dennis, T. A. Lograsso, and R. W. McCallum, *J. Appl. Phys.* **97**, 10M516 (2005).
  - <sup>7</sup> S. H. Song, J. E. Snyder, D. Wu, T. A. Lograsso, K. W. Dennis, R. W. McCallum, Y. Janssen, and D. C. Jiles, *IEEE Trans. Magn.* **41**, 3499 (2005).
  - <sup>8</sup> J. C. Tolédano, R. S. Berry, P. J. Brown, A. M. glazer, R. Metselaar, D. Pandey, J. M. Perez-Mato, R. S. Roth, and S. C. Abrahams, *Acta Cryst. A* **57**, 614 (2001).
  - <sup>9</sup> Z. Fisk and J. P. Remeika, in *Handbook on the Physics and Chemistry of Rare Earths*, edited by K. A. Gschneidner, Jr. and L. Eyring (North-Holland, Amsterdam, 1989), vol. 12.
  - <sup>10</sup> P. C. Canfield and Z. Fisk, *Philos. Mag. B* **65**, 1117 (1992).
  - <sup>11</sup> P. C. Canfield and I. R. Fisher, *J. Cryst. Growth* **225**, 155 (2001).
  - <sup>12</sup> Y. Janssen, M. Angst, K. W. Dennis, R. W. McCallum, and P. C. Canfield, *J. Cryst. Growth* **285**, 670 (2005).
  - <sup>13</sup> Y. Mozharivskyj, unpublished.
  - <sup>14</sup> B. Hunter, Lhpm-rietica, [www.rietica.org](http://www.rietica.org).
  - <sup>15</sup> A. Le Bail, H. Duroy, and J. L. Fourquet, *Mater. Res. Bull.* **23**, 447 (1988).
  - <sup>16</sup> O. I. Bodak and E. I. Hladyshevsky, in *Pearson's Handbook Desk Edition Crystallographic Data for Intermetallic Phases*, edited by P. Villars (ASM International, Materials Park, Ohio, 1997), vol. 1, p. 1199.
  - <sup>17</sup> E. Morosan, S. L. Budko, and P. C. Canfield, *Phys. Rev. B* **72**, 014425 (2005).
  - <sup>18</sup> A. Arrott, *Phys. Rev.* **108**, 1394 (1957).
  - <sup>19</sup> B. Barbara, C. Bécle, R. Lemaire, and D. Paccard, *J. Phys. C* **1**, 299 (1971).
  - <sup>20</sup> T. Egami and C. D. Graham, *J. Appl. Phys.* **42**, 1299 (1971).
  - <sup>21</sup> J. J. van den Broek and H. Zijlstra, *IEEE Trans. Magn.* **7**, 226 (1971).
  - <sup>22</sup> B. Barbara and M. Uehara, *IEEE Trans. Magn.* **12**, 997 (1976).
  - <sup>23</sup> O. Tegus, Y. Janssen, E. Brück, A. A. Menovsky, F. R. de Boer, and K. H. J. Buschow, *J. Alloys Compd.* **317**, 459 (2001).
  - <sup>24</sup> L. J. de Jongh and A. R. Miedema, *Adv. Phys.* **23**, 1 (1974).
  - <sup>25</sup> Y. Janssen, J. C. P. Klaasse, E. Brück, F. R. de Boer, K. H. J. Buschow, J. Kamarád, and N. V. Kudrevatykh, *Physica B* **319**, 59 (2002).
  - <sup>26</sup> Y. Janssen et al., unpublished.
  - <sup>27</sup> A. Llobet, unpublished.